Strongly bound Mott-Wannier excitons in GeS and GeSe monolayers

Lidia C. Gomes,[1] P. E. Trevisanutto,[1,2] A. Carvalho,[1] A. S. Rodin,[1] and A. H. Castro Neto[1]
[1]*Graphene Research Centre and CA2DM, National University of Singapore, Singapore 117542, Singapore*
[2]*Singapore Synchrotron Light Source, National University of Singapore, 5 Research Link, Singapore 117603, Singapore*
(Received 19 July 2016; revised manuscript received 14 September 2016; published 17 October 2016)

The excitonic spectra of single-layer GeS and GeSe are predicted by *ab initio* GW and Bethe-Salpeter equation calculations. G_0W_0 calculations for the band structures find a fundamental band gap of 2.85 eV for GeS and 1.70 eV for GeSe monolayer. However, excitons are tightly bound, specially in GeS at the Γ point, where the quasiparticle interactions are so strong that they shift the Γ exciton peak energy into the visible range and below the off-Γ exciton peak. The lowest energy excitons in both materials are excited by light along the zigzag direction and have exciton binding energies of 1.05 and 0.4 eV, respectively; but despite the strong binding, the calculated binding energies are in agreement with a Mott-Wannier model.

DOI: 10.1103/PhysRevB.94.155428

I. INTRODUCTION

The excitonic properties of two-dimensional (2D) semiconductors have been revealed to be fundamentally different from those of bulk semiconductors. In the 2D limit, the electron and hole experience reduced Coulomb screening as the dielectric environment changes abruptly from the layer to the vacuum [1–4]. Additionally, the confinement of the electron and hole to the plane also contributes to increasing the exciton binding energy. As a result, the optical properties of 2D semiconductors such as transition metal dichalcogenides, phosphorene, and group-IV monochalcogenides are dominated by excitonic effects. Thus, the use of 2D materials for optoelectronic applications requires a deeper understanding of the excitonic properties.

A few experimental studies to date have measured the exciton binding energies of monolayer MoS_2, WS_2, $MoSe_2$, and WSe_2 to be in the range of 0.2–0.8 eV [5–9], even though the values for isolated monolayers are expected, according to theory, to be around 1 eV [10,11]. Another outcome of the nonlocal dielectric screening is that the energy level ordering for the exciton $1s$, $2s$, $2p$, etc., states differs from a hydrogenic Rydberg series [6,12]. In nearly neutral monolayer samples of semiconducting transition metal dichalcogenides, other quasiparticles (QPs) have been observed, including negative and positively charged trions [9,13,14] and biexcitons [13]. Such abundance of excitonic effects has no parallel in 3D systems.

In phosphorene, excitons were also found to be strongly bound, with an exciton binding energy of 0.8–0.9 eV [15,16]. But different from transition metal dichalcogenides, phosphorene has in-plane anisotropy, resulting in nearly unidimensional exciton wave functions [17], such that light emitted upon recombination of the lowest energy exciton is linearly polarized along the light effective mass direction.

Group-IV monochalcogenides assume a structure similar to that of black phosphorus, and therefore marked anisotropy of the optical properties is also expected. However, even though determining band-gap values and optical absorption thresholds and identifying bound excitons are essential measures for the design of optoelectronic devices, determination of the number of layers [18], and optical detection of the ferroelectric and ferroelastic state [19–21], the optical properties of group-IV monochalcogenide monolayers are still the object of discussion [22–24].

In this article, we predict both the GW quasiparticle band structures and the absorption spectra of the group-IV monochalcogenide monolayers GeS and GeSe from first principles, highlighting the large exciton binding energy of GeS. In order to calculate the two-body electron-hole (e-h) Green's function, we have utilized the *ab initio* many-body perturbation theory approach, the Bethe-Salpeter equation (BSE) on top of GW self-energy corrections (GW-BSE) [25]. In addition, we have analyzed the suitability of the Hyde, Scuseria, and Ernzerhof (HSE) hybrid density functional [26] comparing the density functional theory (DFT) and GW band structures. Our results display the presence of bound and localized excitons in both GeS and GeSe monolayers (with the binding exciton energies 1 and 0.4 eV, respectively). The Mott-Wannier model [16] binding energies are in agreement with the GW-BSE values. Moreover, we have determined the exciton binding energy trends for both GeS and GeSe in the presence of substrate dielectric constants. The computational details are provided in Sec. II, whereas the results are displayed and discussed in Sec. III. In Sec. IV, conclusions are discussed.

II. COMPUTATIONAL DETAILS

We use first-principles calculations to obtain the optimized structure and electronic bands of GeS and GeSe monolayers. A first-principles approach is employed based on Kohn-Sham density functional theory (KS-DFT) [27], as implemented in the QUANTUM ESPRESSO code[28]. The exchange-correlation energy are described by the generalized gradient approximation (GGA) using the PBE [29] functional, and the interactions between valence and core electrons are described by the Troullier-Martins pseudopotentials [30]. The Kohn-Sham (KS) orbitals are expanded in a plane-wave basis with a cutoff energy of 70 Ry. The Brillouin zone (BZ) is sampled using a Γ-centered $10\times10\times1$ grid, following the scheme proposed by Monkhorst-Pack (MP) [31]. Structural optimization is performed with a very stringent tolerance of 0.001 eV/Å. In parallel, the HSE hybrid exchange-correlation functional [26] is used to estimate the energy band gap, which is well known to be underestimated by standard DFT exchange-correlation functionals, including the generalized gradient approximations.

The supercells are periodic in the monolayer plane and large vacuum regions (> 10 Å) are included to impose periodic boundary conditions in the perpendicular direction. Convergence tests were performed for the vacuum thickness, and the values used are enough to avoid spurious interaction between neighboring images.

Subsequently, the KS one-electron energies are corrected with the G_0W_0 (*one-shot*) self-energy corrections Σ. These calculations are performed on top of DFT-PBE ground state ones as implemented in BERKELEYGW code [32]. The BZ is sampled with a 32×32×1 MP k-point mesh grid. The convergence is achieved with 500 unoccupied states with a slab plane (xy) truncation of the bare Coulomb potential.

The absorption spectrum is calculated as the imaginary part of the macroscopic dielectric function $\epsilon_M(\omega)$. Starting from the GW-Σ corrections, the electron-hole (e-h) interactions are then included by using the BSE for the two-particle correlation function L. Our GW-BSE calculations are restricted to the Tamm-Dancoff approximation which provides good results for semiconductors. The BSE kernel is evaluated first on a coarse k-grid (32×32×1) and then interpolated onto a finer grid (64×64×1).

III. RESULTS

A. Band structures

The electronic band structure of bulk GeS and GeSe have been discussed in previous theoretical works, where *ab initio* calculations indicate (underestimated) indirect gaps of 1.2 and 0.6 eV, respectively, at the DFT-GGA level [22]. More accurate results are achieved with the HSE hybrid DFT functional and G_0W_0 approximation, and the corrected gaps agree well with available experimental data. For GeS, for example, theory indicates gaps between 1.53 and 1.81 eV, in close agreement with experimental values, in the range 1.70–1.96 eV for the conduction gap after extrapolation to $T = 0$ [33–35]. The spread in experimental values for conduction and optical gaps makes an estimate of the exciton binding energy difficult to obtain, but places a higher bound at 0.3 eV.

Single-layer GeS preserves the indirect gap character (Fig. 1), with the conduction band minimum localized at a point V_y along the Γ-Y line of the Brillouin zone and the valence band maximum (VBM) at a point V_x along Γ-X, the latter very close in energy to a second maximum at Γ. Monolayer GeSe changes from indirect to direct gap along Γ-X. As discussed in Ref. [22], the corrections introduced by the hybrid functional result just in an increase of the gap energy, given by a rigid shift of the bands, while their dispersions are preserved. The minimum indirect and direct gaps of 2.45 and 1.79 eV are calculated at the HSE level for GeS and GeSe, respectively (Table I).

TABLE I. Gap energies for DFT-GGA, HSE, and G_0W_0 methods.

	Fundamental band gap		
	DFT-GGA	HSE	G_0W_0
GeS	1.70	2.45	2.85
GeSe	1.14	1.79	1.70

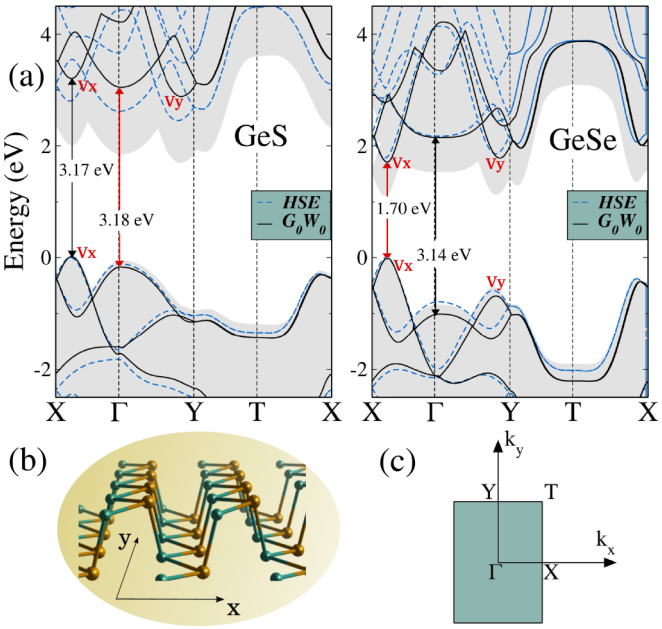

FIG. 1. (a) Electronic structure of GeS and GeSe monolayers calculated by GGA (full gray background), HSE (dashed blue lines), and GW (full black lines) methods. The direct transitions shown by the red arrows give rise to the excitons of highest binding energies. (b) The structure of the monolayers showing the armchair and zigzag directions placed along the x and y axis, respectively. (c) BZ with the high symmetry points.

In Fig. 1, the G_0W_0 corrections to the band structure are shown. Similar to the HSE results, the conduction and valence bands are rigidly shifted away from each other, with the minima and maxima located at the same positions in the high symmetry lines of the BZ as the DFT-GGA and HSE methods. The resulting indirect energy gap of 2.85 eV and direct gap of 1.70 eV for GeS and GeSe, respectively, show differences of 0.4 and 0.09 eV from the predicted values by the HSE approximation to the exchange-correlation energy with an overall good agreement in the band values and band dispersions. In GeS, most importantly, the direct band gap values at Γ and V_x point are nearly identical for all three methods.

B. Absorption spectra

In Fig. 2, we present the absorption spectra of single-layer GeS calculated in the GW-random-phase approximation (GW-RPA) (labeled "without e-h interactions") and GW-BSE approach ("with e-h interactions"). Due to anisotropy, the absorption spectrum along x (armchair direction) considerably differs from the polarization along y (zigzag direction). In the armchair direction, when the e-h interactions are not included, the first two peaks are placed at ∼ 3.17 and 3.18 eV, the values of the direct band gaps at Γ and V_x. The scenario changes in the GW-BSE framework: two intense exciton peaks are present at 2.2 and 2.6 eV, below the indirect G_0W_0 gap of 2.85 eV. These two excitons are still originated from critical points but the e-h interactions induce different intensity, and have different binding energies. The first exciton at 2.2 eV

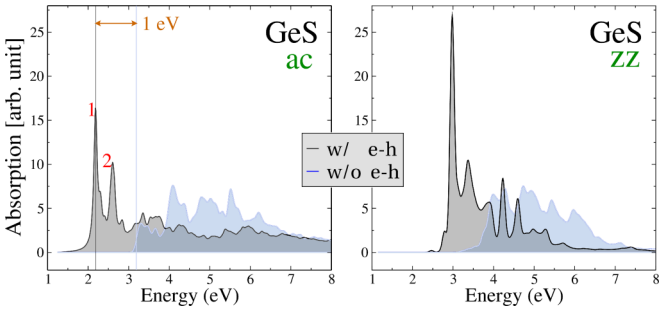

FIG. 2. Absorption spectra of GeS monolayer with (gray spectrum) and without (blue spectrum) electron-hole interactions for light polarized along zigzag (zz) and armchair (ac) in-plane directions. Two exciton states (peaks 1 and 2) are formed inside the G_0W_0 gap along x. Peak 1 arises from direct transitions at Γ, while peak 2 is due to direct transitions at the V_x valleys (along the Γ-X direction).

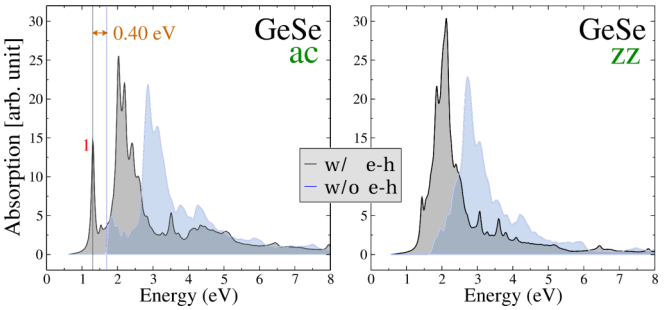

FIG. 3. Same as Fig. 2, but for the GeSe monolayer. There is one excitonic state along x (peak 1), due to a direct transition at the V_x valleys (along the Γ-X direction).

shows a very strong binding energy of $E_b = 1$ eV and is assigned to direct transitions at Γ. The second exciton peak (of lower intensity) is originated from the direct transitions between the valleys V_x and shows a much weaker binding energy of $E_b = 0.5$ eV. This result confirms the qualitative hydrogen-like picture in which the higher binding energies arise from the higher effective mass at Γ with respect to V_x (the numerical values in Table II). In contrast, in the zigzag case, the top valence and bottom conduction band transitions at V_x and Γ points are very attenuated by the dipole coupling term (as displayed at the GW-RPA level). The GW-BSE absorption spectrum calculations show strong excitonic effects that lead single-particle transitions with energies higher than the band gap to the continuum of the bottom of the conduction band. Excitons living in the band gap are almost suppressed.

In the GeSe monolayer, absorption spectrum calculations (Fig. 3) provide different outcomes. As far as the armchair direction is concerned, in the absorption spectra calculated with the GW-RPA the first peak is at 1.70 eV, originated at V_x. This is well separated from the most intense peak at 3.14 eV, originating at the Γ point. In GW-BSE, the only exciton in the fundamental band gap is placed at 1.30 eV, with a binding energy $E_b = 0.4$ eV. In the zigzag direction, the excitonic effects determine a general red shift of the one-particle excited states with an increase in intensity of the continuum of the transitions.

In order to better understand the nature of the first peak excitons in armchair directions in GeS and GeSe monolayers, the normalized squared electron-hole wave functions (e-h WF)

TABLE II. Effective masses of electrons (m_e^*/m_0) and holes (m_h^*/m_0) of valleys located at Γ and at the V_x valley (along the Γ-X direction), for the x and y in-plane directions.

	V_x				Γ			
	m_e^*/m_0		m_h^*/m_0		m_e^*/m_0		m_h^*/m_0	
	x	y	x	y	x	y	x	y
GeS	0.27	−0.50	0.23	−0.46	0.57	−1.99	0.65	−1.39
GeSe	0.20	−0.22	0.17	−0.20	1.28	−2.75	2.83	−4.17

$\Psi(\mathbf{r_e}, \mathbf{r_h},)$ are shown in Fig. 4. The hole is placed in the center (blue spot). The plot sizes correspond to a 16×16 unit cell. It is clear that the low-energy exciton is more spatially localized in GeS than in GeSe, as should be expected by its higher E_b and more ionic behavior of sulfur atoms with respect to selenium atoms which reduce the electronic screening [36]. Conversely to GeS, in GeSe the envelope of the e-h density displays a modulation along the x axis, occurring on a length scale of ≈3 unit cells.

C. Mott-Wannier model

The GW-BSE framework used so far to investigate the optical properties of GeS and GeSe monolayers provides information on excitonic properties of the isolated 2D systems. Nevertheless, to further clarify the nature of the excitons described above (if Frenkel or Mott-Wannier) and to evaluate the substrate effects in the binding energies, we have applied the model in Ref. [16] for excitons in anisotropic 2D semiconducting crystals.

When dealing with 2D materials, one must exercise caution as the Coulomb term is replaced by the Keldysh-like potential due to the in-plane screening. The potential ϕ_{2D} felt by an electron in a 2D dielectric was obtained in Ref. [2] for a 2D sheet in vacuum and extended in Ref. [16] including the effects of a substrate bulk dielectric. For the latter case, the potential ϕ_{2D} created by a charge q, has the form

$$\phi_{2D}(r) = \frac{\pi q}{2\kappa r_0}\left[H_0\left(\frac{r}{r_0}\right) - Y_0\left(\frac{r}{r_0}\right)\right]. \quad (1)$$

$H_0(r)$ and $Y_0(r)$ are Struve and Bessel functions, respectively, and $r_0 = 2\pi\xi/\kappa$ is a length scale depending on the 2D polarizability ξ and on the substrate dielectric constant ϵ through $\kappa = (1+\epsilon)/2$.

From the asymptotic behavior of $H_0(r)$ and $Y_0(r)$ it is determined that at large r, the ϕ_{2D} interaction follows the usual $1/r$ form, while at small distances it diverges logarithmically [1–4]. Since the logarithmic well is more gradual than $1/r$, this results in substantially smaller binding energies.

Once the correct potential is chosen, it is important to keep in mind that the reduction of the two-body exciton problem to a single-body central potential problem is only applicable to Mott-Wannier excitons where the wave function is much larger than the lattice constant. The reason behind this requirement is

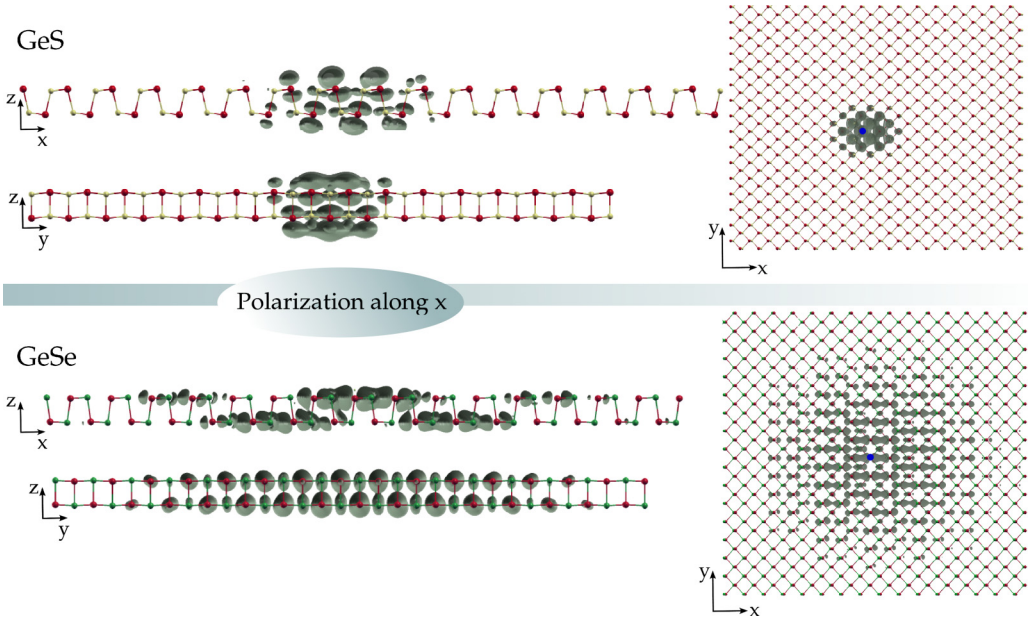

FIG. 4. Normalized squared exciton wave function ($Å^{-2}$) of excitons in GeS and GeSe for incident light polarized along the in-plane x direction. The plot size corresponds to 16×16 lattice spacings.

the fact that the potential (1) treats the system as a continuous medium. With these considerations, it is possible to determine exciton binding energies of 2D anisotropic materials, with and without substrate effects, as detailed in Ref. [16].

The dependence of the exciton binding energies on the substrate dielectric constant κ, for single-layer GeS and GeSe, are presented in the plot in Fig. 5, for κ ranging from 1 to 5. For the case of isolated layers, for which $\kappa = 1$, the model gives $E_b = 1.10$ and 0.45 eV for GeS and GeSe, respectively. This result is in fairly good agreement with the values obtained with our *ab initio* GW-BSE calculations, confirming that these excitons are of Mott-Wannier character.

Screening effects introduced by the substrate decrease the binding energies with increasing κ. As an example, a reasonable choice is to consider the layers deposited on a SiO_2 substrate ($\kappa \approx 2.4$). In this case, the exciton binding energies are reduced to 0.60 and 0.22 eV for GeS and GeSe, placing phosphorene in the middle way of these two materials,

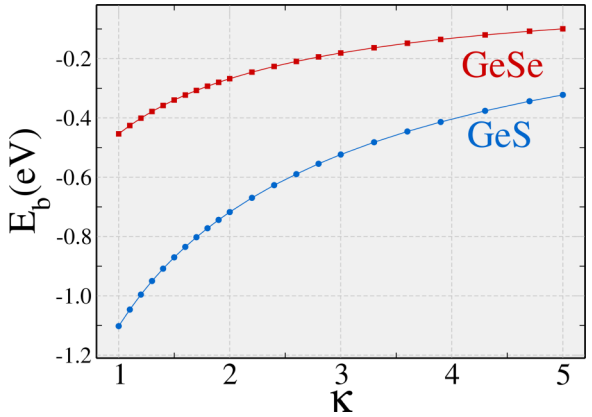

FIG. 5. Exciton binding energy of GeS and GeSe monolayers as a function of the substrate dielectric constant $\kappa = (1 + \epsilon)/2$.

with an exciton binding energy of 0.4 eV for the same substrate [16].

IV. CONCLUSIONS

Quasiparticle band structure and excitonic properties of orthorhombic two-dimensional GeS and GeSe are investigated by first-principles calculations. The G_0W_0 formalism indicates that 2D GeS is a indirect gap material with an energy gap of 2.85 eV, while 2D GeSe is characterized by a minimum direct gap of 1.70 eV.

However, the optical spectra of both materials is dominated by excitonic effects. GeS Γ-point excitons have a remarkably large binding energy of 1 eV, shifting the optical absorption threshold to 2.2 eV, in the visible range (rather than at 3.17 eV, in the near-ultraviolet region, as expected from the quasiparticle gap). Additionally, the two gap excitons at Γ and at the V_x valley (along the Γ-X direction) couple with light polarized along the x direction. Thus, between 2.2 and 2.6 eV, optical absorption is polarized.

For GeSe, the only exciton in the gap, with a binding energy of 0.4 eV, corresponds to the V_x valley. The binding energy of this exciton is more robust to external dielectric screening than in GeS. Despite their strong binding, exciton binding energies are found to be in agreement with a 2D Mott-Wannier model [16].

ACKNOWLEDGMENTS

The first-principles calculations were carried out on the GRC high-performance computing facilities. This work was supported by the National Research Foundation, Prime Minister Office, Singapore, under its Medium Sized Centre Programme and by the CRP award "Novel 2D materials with tailored properties: beyond graphene" (Grant No. R-144-000-295-281).

[1] L. V. Keldysh, Coulomb interaction in thin semiconductor and semimetal films, JETP Lett. **29**, 658 (1979).

[2] P. Cudazzo, I. V. Tokatly, and A. Rubio, Dielectric screening in two-dimensional insulators: Implications for excitonic and impurity states in graphene, Phys. Rev. B **84**, 085406 (2011).

[3] T. C. Berkelbach, M. S. Hybertsen, and D. R. Reichman, Theory of neutral and charged excitons in monolayer transition metal dichalcogenides, Phys. Rev. B **88**, 045318 (2013).

[4] A. Castellanos-Gomez, L. Vicarelli, E. Prada, J. O. Island, K. L. Narasimha-Acharya, S. I. Blanter, D. J. Groenendijk, M. Buscema, G. A. Steele, J. V. Alvarez, H. W. Zandbergen, J. J. Palacios, and H. S. J. van der Zant, Isolation and characterization of few-layer black phosphorus, 2D Mater. **1**, 025001 (2014).

[5] C. Zhang, A. Johnson, C.-L. Hsu, L.-J. Li, and C.-K. Shih, Direct imaging of band profile in single layer MoS_2 on graphite: Quasiparticle energy gap, metallic edge states, and edge band bending, Nano Lett. **14**, 2443 (2014).

[6] Z. Ye, T. Cao, K. O'Brien, H. Zhu, X. Yin, Y. Wang, S. G. Louie, and X. Zhang, Probing excitonic dark states in single-layer tungsten disulphide, Nature **513**, 214 (2014).

[7] M. M. Ugeda, A. J. Bradley, S.-F. Shi, F. H. da Jornada, Y. Zhang, D. Y. Qiu, S.-K. Mo, Z. Hussain, Z.-X. Shen, F. Wang, S. G. Louie, and M. F. Crommie, Giant bandgap renormalization and excitonic effects in a monolayer transition metal dichalcogenide semiconductor, Nat. Mater. **13**, 1091 (2014).

[8] G. Wang, X. Marie, I. Gerber, T. Amand, D. Lagarde, L. Bouet, M. Vidal, A. Balocchi, and B. Urbaszek, Giant Enhancement of the Optical Second-Harmonic Emission of WSe_2 Monolayers by Laser Excitation at Exciton Resonances, Phys. Rev. Lett. **114**, 097403 (2015).

[9] B. Zhu and X. Cui Xi Chen, Exciton binding energy of monolayer WS_2, Sci. Rep. **5**, 9218 (2015).

[10] H.-P. Komsa and A. V. Krasheninnikov, Effects of confinement and environment on the electronic structure and exciton binding energy of MoS_2 from first principles, Phys. Rev. B **86**, 241201 (2012).

[11] D. Y. Qiu, F. H. da Jornada, and S. G. Louie, Optical Spectrum of MoS_2: Many-Body Effects and Diversity of Exciton States, Phys. Rev. Lett. **111**, 216805 (2013).

[12] A. Chernikov, T. C. Berkelbach, H. M. Hill, A. Rigosi, Y. Li, O. B. Aslan, D. R. Reichman, M. S. Hybertsen, and T. F. Heinz, Exciton Binding Energy and Nonhydrogenic Rydberg Series in Monolayer WS_2, Phys. Rev. Lett. **113**, 076802 (2014).

[13] J. Shang, X. Shen, C. Cong, N. Peimyoo, B. Cao, M. Eginligil, and T. Yu, Observation of excitonic fine structure in a 2d transition-metal dichalcogenide semiconductor, ACS Nano **9**, 647 (2015).

[14] K. F. Mak, K. He, C. Lee, G. H. Lee, J. Hone, T. F. Heinz, and J. Shan, Tightly bound trions in monolayer MoS_2, Nat. Mater. **12**, 207 (2013).

[15] Vy Tran, R. Soklaski, Y. Liang, and L. Yang, Layer-controlled band gap and anisotropic excitons in few-layer black phosphorus, Phys. Rev. B **89**, 235319 (2014).

[16] A. S. Rodin, A. Carvalho, and A. H. Castro Neto, Excitons in anisotropic two-dimensional semiconducting crystals, Phys. Rev. B **90**, 075429 (2014).

[17] X. Wang, A. M Jones, K. L. Seyler, Vy Tran, Y. Jia, H. Zhao, H. Wang, L. Yang, X. Xu, and F. Xia, Highly anisotropic and robust excitons in monolayer black phosphorus, Nat. Nanotechnol. **10**, 517 (2015).

[18] J. R. Brent, D. J. Lewis, T. Lorenz, E. A. Lewis, N. Savjani, S. J. Haigh, G. Seifert, B. Derby, and P. OBrien, Tin(ii) sulfide (SnS) nanosheets by liquid-phase exfoliation of herzenbergite: IV–VI main group two-dimensional atomic crystals, J. Am. Chem. Soc. **137**, 12689 (2015).

[19] M. Wu and X. C. Zeng, Intrinsic ferroelasticity and/or multiferroicity in two-dimensional phosphorene and phosphorene analogues, Nano Lett. **16**, 3236 (2016).

[20] H. Wang and X. Qian, Two-dimensional multiferroics: Ferroelasticity, ferroelectricity, domain wall, and potential mechano-opto-electronic applications, arXiv:1606.04522.

[21] P. Z. Hanakata, A. Carvalho, D. K. Campbell, and H. S. Park, Memory effects in monolayer group-IV monochalcogenides, Phys. Rev. B **94**, 035304 (2016).

[22] L. C. Gomes and A. Carvalho, Phosphorene analogues: Isoelectronic two-dimensional group-IV monochalcogenides with orthorhombic structure, Phys. Rev. B **92**, 085406 (2015).

[23] G. A. Tritsaris, B. D. Malone, and E. Kaxiras, Optoelectronic properties of single-layer, double-layer, and bulk tin sulfide: A theoretical study, J. Appl. Phys. **113**, 233507 (2013).

[24] G. Shi and E. Kioupakis, Anisotropic spin transport and strong visible-light absorbance in few-layer SnSe and GeSe, Nano Lett. **15**, 6926 (2015).

[25] G. Onida, L. Reining, and A. Rubio, Electronic excitations: Density-functional versus many-body Green's-function approaches, Rev. Mod. Phys. **74**, 601 (2002).

[26] K. Hummer, J. Harl, and G. Kresse, Heyd-Scuseria-Ernzerhof hybrid functional for calculating the lattice dynamics of semiconductors, Phys. Rev. B **80**, 115205 (2009).

[27] W. Kohn and L. J. Sham, Self-consistent equations including exchange and correlation effects, Phys. Rev. **140**, A1133 (1965).

[28] P. Giannozzi *et al.*, Quantum espresso: A modular and open-source software project for quantum simulations of materials, J. Phys.: Condens. Matter **21**, 395502 (2009).

[29] J. P. Perdew, K. Burke, and M. Ernzerhof, Generalized Gradient Approximation Made Simple, Phys. Rev. Lett. **77**, 3865 (1996).

[30] N. Troullier and J. L. Martins, Efficient pseudopotentials for plane-wave calculations, Phys. Rev. B **43**, 1993 (1991).

[31] H. J. Monkhorst and J. D. Pack, Special points for Brillouin-zone integrations, Phys. Rev. B **13**, 5188 (1976).

[32] J. Deslippe, G. Samsonidze, D. A. Strubbe, M. Jain, M. L. Cohen, and S. G. Louie, BERKELEYGW: A massively parallel computer package for the calculation of the quasiparticle and optical properties of materials and nanostructures, Comput. Phys. Commun. **183**, 1269 (2012).

[33] R. Eymard and A. Otto, Optical and electron-energy-loss spectroscopy of GeS, GeSe, SnS, and SnSe single crystals, Phys. Rev. B **16**, 1616 (1977).

[34] J. H. Haritonidis and D. S. Kyriakos, Conductivity of layered GeS at low temperatures connected with the presence of planar defects, Semicond. Sci. Technol. **4**, 365 (1989).

[35] B. D. Malone and E. Kaxiras, Quasiparticle band structures and interface physics of SnS and GeS, Phys. Rev. B **87**, 245312 (2013).

[36] M. Dvorak, S.-H. Wei, and Z. Wu, Origin of the Variation of Exciton Binding Energy in Semiconductors, Phys. Rev. Lett. **110**, 016402 (2013).